chemosensors

MDPI

Article

Potentiometric Sensor System with Self-Calibration for Long-Term, In Situ Measurements

Zhehao Zhang [1], Elena Boselli [1] and Ian Papautsky [1,2,*]

[1] Department of Biomedical Engineering, University of Illinois Chicago, Chicago, IL 60607, USA
[2] NSF Center for Advanced Design and Manufacturing of Integrated Microfluidics (CADMIM), Chicago, IL 60607, USA
* Correspondence: papauts@uic.edu; Tel.: +1-312-413-3800

Abstract: We built an integrated solid-contact ion-selective electrode (SCISE) system with the functionality of self-calibration. A multiplexed SCISE sensor (K^+ and NO_3^- vs. Ag/AgCl) was fabricated on printed-circuit board (PCB) substrates and was subsequently embedded into a microfluidic flow cell for self-calibration and flow-through analysis. A PCB circuit that includes modules for both sensor readout and fluid control was developed. The sensors showed a fast and near-Nernstian response (56.6 for the K^+ electrode and −57.4 mV/dec for the NO_3^- electrode) and maintained their performance for at least three weeks. The sensors also showed a highly reproducible response in an automated two-point calibration, demonstrating the potential for in situ monitoring. Lastly, the sensor system was successfully applied to measure mineral nutrients in plant sap samples.

Keywords: ion-selective electrode; printed circuit board; in situ measurement; potentiometry; self-calibration

Citation: Zhang, Z.; Boselli, E.; Papautsky, I. Potentiometric Sensor System with Self-Calibration for Long-Term, In Situ Measurements. *Chemosensors* **2023**, *11*, 48. https://doi.org/10.3390/chemosensors11010048

Academic Editors: Iulia Gabriela David and Dana Elena Popa

Received: 13 December 2022
Revised: 30 December 2022
Accepted: 1 January 2023
Published: 5 January 2023

1. Introduction

Ion-selective electrodes (ISE) are commonly used to develop fast, portable, and cost-effective analytical devices. Such devices have found wide applications in point-of-care testing and medicine [1–4], wearables [5,6], agriculture [7], and environmental monitoring [8,9]. In recent years, the development of solid contact (SC) materials as ion-to-electron transducers has driven the field towards next-generation sensors that are miniaturized, rugged, and calibration- and maintenance-free [10]. Despite the progress, the majority of these solid contact ISEs (SCISEs) still need to be calibrated as their conventional counterparts with an inner filling solution.

Sensors are calibrated to correct for sensitivity loss, baseline drift, and inter-sensor variability. Usually, calibration is performed by the user before and/or after each measurement. Although manual calibration may be sufficient for single-use sensors, it is cumbersome for recurring and continuous measurements; moreover, it is not feasible for in situ measurements in agricultural, environmental, or geochemical analysis where sensors need to be deployed in the field and work autonomously. In these scenarios, automatic calibration at the point of need not only saves time and effort but ensures the accuracy and precision of measurement.

Only a few potentiometric sensor systems with a self-calibration function have been reported to date [2,8,9,11]. They typically employ a flow cell that introduces calibrating reagents to the sensor using fluidic components (e.g., pumps and valves) and corresponding fluid-control modules. In addition, such flow cell arrangement allows for electrode cleaning and sample pretreatment and often leads to lower detection limits than the stationary approach [12,13]. For example, the commercial Abbott i-STAT blood analyzer performs on-site calibration of the sensor through a series of pumping and valving mechanisms [2]; however, since the sensor was intended for single use, its calibration was limited to once per test. More recently, Cuatero et al. [8,9] developed a submersive probe based on a

SCISE-embedded flow cell to monitor seawater in hourly measurements followed by a one-point calibration. However, the sensor readout and fluid control relied on dedicated commercial instruments, which significantly increased the cost and complexity of the system; in addition, the proprietary nature of these commercial systems does not allow them to be easily transferred into other applications. Therefore, a more integrated, open-source sensor system is highly desired, especially for long-term, in situ measurements.

In this work, we developed a potentiometric sensor system with self-calibration capability by integrating a multiplexed SCISE sensor with electronics and fluidic components. Importantly, both the sensor readout and fluid control modules are combined into a single PCB circuit, which makes the system cost-effective, portable, and adaptable. Both the circuit and the multiplexed sensor (K^+ and NO_3^- sensors and Ag/AgCl reference) were fabricated using printed-circuit board (PCB) technology [14]. The sensor was further embedded into a microfluidic flow cell and its potentiometric response was characterized under different flow conditions. To prepare the sensor for future in situ measurements, we then demonstrated the long-term operation and automated two-point calibration. Finally, the sensor was validated with plant sap samples.

2. Materials and Methods

2.1. Materials and Reagents

Mesoporous carbon black (MCB, average pore diameter 6.4 nm), potassium ionophore I (valinomycin), potassium tetrakis(4-chlorophenyl)-borate (KTPB), tridodecylmethylammonium nitrate (TDDMA-NO_3), polyvinyl chloride (PVC, high molecular weight), tetrahydrofuran (THF), and 2-nitrophenyl octyl ether (NPOE) were purchased from Sigma Aldrich (MA, US). Salts of NaCl, KNO_3, KCl were purchased from Fisher Scientific. Silver plating solution (Technic Silver Cyless RTU) was purchased from Technic Inc. All chemicals were of analytical or industrial grade. Deionized (DI) water was used to prepare all aqueous solutions. Double-sided (#9474LE) and single-sided (#9964) adhesive tapes were obtained from 3M. Tygon tubing (0.02″ ID × 0.06″ OD) was purchased from Cole-Parmer.

Suspension of mesoporous carbon black (MCB) was prepared by adding 45 mg MCB and 5 mg PVC as binder into 2 mL THF. Prior to each use, the suspension was vortexed for 30 s, sonicated for 1 h, and then vortexed again for 30 s to disperse the nanoparticles. The K^+ ISE cocktail was prepared by mixing 22.2 mg K^+ ionophore I, 7.0 mg KTPB, 320 mg PVC, and 660 µL NPOE into 10 mL THF and stirring until all components were fully dissolved. For the NO_3^- cocktail, 10 mg TDDMA-NO_3, 330 mg PVC, and 660 µL NPOE were subsequently added to 10 mL THF and stirred until fully dissolved.

2.2. Sensor System

The potentiometric sensor system consists of the multiplexed SCISE sensor and a PCB circuit to control fluidics and perform both sensor readout and calibration. This is schematically illustrated in Figure 1A. A buffer amplifier (LTC6079, Analog Devices, Wilmington, MA, USA) and a 3-channel, 16-bit ADC (analog-to-digital converter, AD7792, Analog Devices) were used to read sensor signals. For fluid control, a DC motor driver based on DRV8830 (Texas Instrument, Dallas, TX, USA) and two DC-DC boost converters based on LTC3122 (Analog Devices) were used to activate pump and valves, respectively. The PCB circuit and the sensor were produced following standard PCB workflow. Briefly, double-sided PCB substrates (FR-4) with connecting traces were designed in CAD software (EasyEDA) and then sent out to a PCB manufacturer for fabrication (Shenzhen JDB Technology, Shenzhen, China). An Arduino circuit (Nano33BLE or Nano33IoT) was used for programming and data transmission (Bluetooth or WiFi) via its microcontroller. The entire circuit (custom PCB + Arduino) can be powered by battery (4.5-21VDC) or USB (3.3VDC).

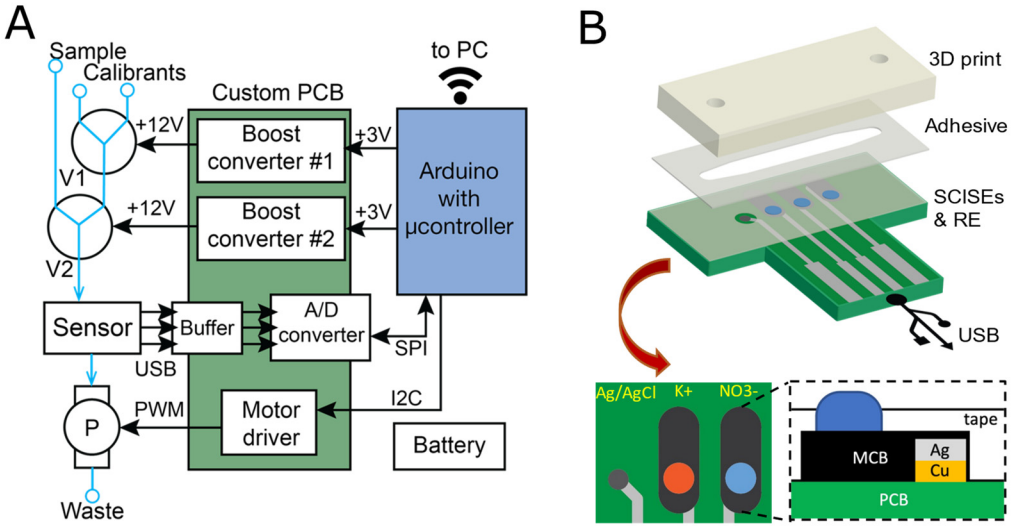

Figure 1. Design of the integrated SCISE sensor system. The system consists of a multiplexed SCISE sensor and a custom PCB for sensor readout and calibration: (**A**) Block diagram of the system illustrates the custom PCB circuit (center) and the supporting fluidic components. Arduino (right side) was used for device control and data transmission. Solenoid valves (V1, V2) and peristaltic pump (P) formed the fluidic circuit (left side). (**B**) Schematic illustration of the multiplexed sensor showing microfluidic integration, sensor layout, and the cross-sectional view of the sensing layers. Note the lateral shift of the ion-selective membrane on top of the mesoporous carbon black (MCB) layer to prevent water layer formation.

Miniaturized peristaltic pump (RP-Q1, H12 × W14 × L30 mm) and solenoid valves (EXAKN-3, φ14.0 × H42.3 mm) were obtained from Takasago Fluidic Systems (Nagoya, Japan). During operation, the pump was placed downstream of the sensor to pull fluid across the sensor, with an adjusted output of 0.2–0.45 mL/min. The 3-way solenoid valves were connected in series and allowed selection of up to 3 reagents.

2.3. Sensor Fabrication

Multiplexed SCISE sensors were prepared based on a process developed previously [14]. The PCB substrates were fabricated using standard PCB technology as described above. In this case, immersion silver was applied as the surface finish. The K^+ and NO_3^- SCISEs were prepared by subsequently drop-casting the MCB suspension (4 µL) and the membrane cocktails (2.8 µL) onto the sensing areas defined on the PCB substrate, using adhesive tapes (3M #9964) for patterning. The sensor structure and layer stacking are illustrated in Figure 1B. The resulting dimensions of the ISEs were 0.06 mm × 1.5 mm (h × w). The ISEs were left to dry in ambient air at room temperature for at least one day before use.

Silver/silver chloride (Ag/AgCl) reference electrodes were prepared by electroplating on the original Ag layer of the PCB, using an industrial plating solution (Technic). To avoid contamination, electroplating was performed before preparing SCISEs. To plate silver, a DC current (−25 µA) was applied for 40 min with a potentiostat (Gamry Reference 600+) and a gold disc (BASi) as counter electrode. After plating, the electrode was cleaned with abundant isopropyl alcohol and DI water to remove organic residues. Then, the electrode was chloridized in 0.1 M KCl by applying a DC current (+ 25 µA) for 20 min, using the same cell setup as silver plating.

2.4. Microchannel Fabrication

The sensor was enclosed into a straight microchannel (17 mm × 2.5 mm × 0.17 mm) constructed by adhesive bonding of a 3D-printed enclosure directly onto the sensor PCB (Figure 1B). The enclosure contained two through-holes as input/output ports of 1.675 mm in diameter to match the OD of Tygon tubing. The enclosure was designed in SolidWorks

and printed using a stereolithography printer (Form 2, Formlabs, Somerville, MA, USA), with a vertical printing orientation (slightly tilted). The printed part was cleaned with isopropyl alcohol and cured in ambient air at room temperature overnight. For better visualization, one side of the printed enclosure was polished using sandpaper (up to 15,000 grit) to produce a transparent surface finish. Bonding of the enclosure to PCB was accomplished using double-sided tape (3M #9474LE), which was patterned in the shape of the channel with a laser cutter (HP2436, Boss Laser, FL). The channel was assembled by hand pressing all the layers with the sensor as the substrate, the tape as the spacer (sidewalls), and the 3D print as the top. After assembly, leakage test was conducted by running continuous flow of dye solution through the channel using a syringe pump (New Era Pump Systems, Inc., Farmingdale, NY, USA), with stepwise increase in flow rate (0.05 to 10 mL/min). At each flow rate, channel integrity was examined visually.

2.5. Sensor Characterization

Potentiometric response of the ISEs was recorded (vs. the electroplated Ag/AgCl) in the microchannel, using either the custom PCB circuit developed here or a dual-channel pH meter (Model 225, Denver Instruments). A series of KNO_3 (10^{-7} to 10^{-1} M) was prepared as the electrolyte standard, with NaCl added to provide constant Cl^- background ($[Cl^-]$ = 10 mM) for the Ag/AgCl reference. For testing hydrodynamic conditions, a constant flow (0.45 mL/min) was driven across the sensor for about 5 min and then the flow was stopped for another 5 min before switching to a higher concentration. At each step, the average sensor response in the last 30 s was used for calibration. For long-term characterization as well as self-calibration, a programmed sequence consisting of 25 s flow period and 60 s static period was implemented, while switching between 10^{-3} and 10^{-2} M KNO_3. At each concentration, the sensor's response was taken by averaging data from the last 10 s of the static period.

Potentiometric response of the electroplated Ag/AgCl electrode was measured against a commercial Ag/AgCl electrode (MW-2030, BASi) in bulk solution (1 mM KNO_3 + 10 mM NaCl), using either the pH meter (Denver Instruments) or a bipotentiostat (WaveDriver 20, Pine Instrument, PA). Data were processed and visualized in LabVIEW, MATLAB, or Arduino IoT Cloud in case of WiFi transmission. At the end of each test, the microchannel was flushed with air and the sensors were stored in dry conditions and against light.

2.6. Plant Sap Test

Xylem sap from maize (*Zea mays*) was collected following the root pressure method described previously [15]. Briefly, plants were either well-watered or not watered 2–3 h prior to collection. Then, an incision was made by surgical blade right above the first stem node to remove the top part. Silicone tubes were inserted into the cut site to collect root exudate. The cut site was rinsed with DI water to remove tissue residues and the first ~100 µL sap was discarded. Collection last for ~4 h, which typically resulted in a sap volume of 1–5 mL per plant. The collected sap was stored at freezer temperature (−20 °C) until further testing.

During testing, sap samples were pre-diluted 10× with a solution of 1 mM KNO_3 + 10 mM NaCl. After an initial conditioning phase (5–10 min), a program of pump and valve actions was implemented such that the sensor was calibrated before and after each sap measurement with standard solutions (1/10 mM KNO_3 + 10 mM NaCl). The EMF value at each step was calculated by averaging the last 10 data points at stopped-flow. Ion concentrations (K^+ and NO_3^-) from the original sample were calculated by $C_{unkown} = (C_{dilute} - 0.9) \times 10$ (mM), where C_{dilute} was the concentration of diluted sample. For testing with commercial K^+ and NO_3^- ISEs (9319BN, 9307BN, ThermoOrion, Waltham, MA, USA), the original sap samples were diluted 10–20× and measured following both 'Direct Calibration' and 'Known Addition' protocols according to the manufacturer [16]. The accuracy of our measurements was calculated by dividing the concentrations measured with our and the commercial sensors.

3. Results and Discussion

3.1. System Design

The key feature of the sensor system is the ability to perform automatic sensor calibrations at low cost and in a small form factor. The fully assembled sensor system is shown in Figure 2A. The 3D-printed enclosure is approx. 8 cm square, and about 5 cm deep; however, the size of the enclosure is primarily driven by the size of the used fluid reservoirs and a much more compact arrangement should be possible, especially with lower volume or external fluid compartments. Instead of relying on external fluid control instruments that are usually bulky and expensive, we integrated flow-control modules into the custom PCB circuit (Figure 2B). The motor driver controls the pump speed via pulse-width modulation (PWM). The boost converters control the switching of valves by stepping up voltage input (+3VDC) to the rated voltage of solenoids (+12VDC) while featuring output disconnect during shutdown to save power. Miniaturized peristaltic pump and solenoid valves were selected due to their compact sizes and lower costs than common syringe pumps and rotary valves. While microfluidic pumps and valves have also been widely developed, they increase the total cost of sensor fabrication and tend to suffer leakage issues [17,18].

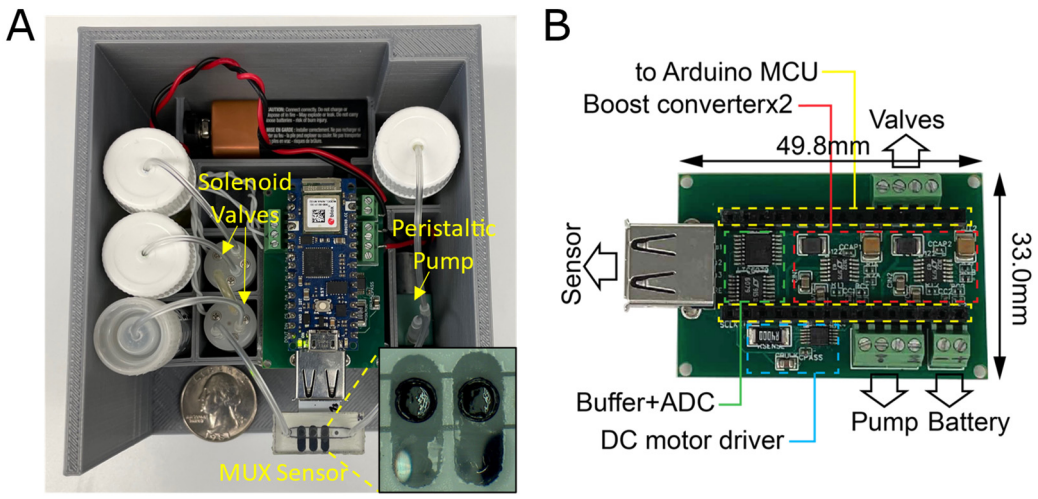

Figure 2. Integrated SCISE sensor system for long-term, in situ measurements: (**A**) Photograph of the fully assembled system. The Arduino board was connected to the custom PCB by stacking. (**B**) Photograph of the custom PCB circuit showing the layout of functional modules.

Power consumption is important for battery-powered devices. The system here draws a current of ~7/30/250 mA, respectively, during default (measuring alone), pumping, and solution switching (when both pump and valve are activated) modes. With a single 9 V battery, the cut-off voltage of the device is found to be ~7.5 V (below which the boost converters could not generate enough current to activate the solenoid valves). Based on these results, we estimate that with a single battery charge the device can continuously run for up to 40 h or about 50 automatic calibrations (see Methods and also below). The operating life can be further extended by using a high-capacity battery such as a power bank.

3.2. Sensor Fabrication and Microfluidic Enclosure

The multiplexed sensor containing SCISEs for K^+ and NO_3^- ions and a Ag/AgCl reference electrode was fabricated on PCB substrates due to the cost-effectiveness of the process and its potential for high-throughput manufacturing. Mesoporous carbon black (MCB) was used as the transducing layer to stabilize the potentiometric response of SCISEs due to its high surface area and good conductivity [14,19]. To suppress the formation of a water layer under the membrane, the ion-selective membranes were shifted laterally from the underlying conducting layer, as shown in Figure 1B, and were discussed in detail in our earlier work [14].

To enable self-calibration capability (and flow-through analysis), the sensor was integrated with a microfluidic flow cell constructed with adhesive tapes and 3D printing. While a variety of microfabrication techniques, such as soft lithography, hot embossing, and injection molding, can be used to make microfluidic channels [20–25], the simplicity and versatility of pressure-sensitive adhesives and 3D printing make them ideal for rapid prototyping of larger microfluidic structures [26,27]. As the spacer layer, the double-coated tape (#9474LE) has proven to be leak-free and chemically inert to the sensor during months of measurement. The 3D-printed top part provided a direct tubing connection via through-holes. Due to the limited resolution of our low-cost 3D printer (~50 µm), it was difficult to consistently print perfectly matched inlets for the tubing and occasional bubbles were introduced at the tubing interface. Nevertheless, when an air-tight interface was formed, the microchannel can sustain flow rates of at least 10 mL/min, which is sufficient for many microfluidic applications and the sensor system herein (where flow rate $\leq$ 0.45 mL/min was used).

3.3. Sensor Performance

A reliable reference electrode is a prerequisite for a stable potentiometric sensor; thus, we first tested the potentiometric response of the electroplated Ag/AgCl electrodes, as shown in Figure 3. The electrodes displayed an average drift of -2.7 ± 0.8 mV (-0.044 mV/min) within the first hour and a baseline reproducibility of 112.8 ± 4.0 mV. Such moderate drift and reproducibility are deemed sufficient for fast analysis, although long-term measurements would require regular calibration. Better performance may be achieved on PCB substrates by electroless silver plating [28] or ink-jet printing [29].

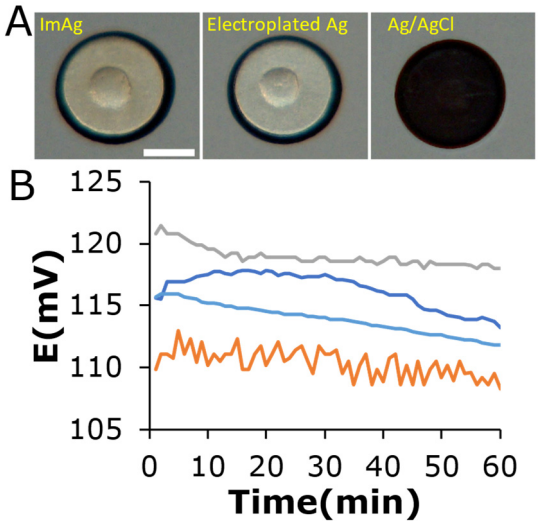

Figure 3. (**A**) Electroplated Ag/AgCl reference electrode. Photographs (left to right) of the original immersion silver layer of PCB, electroplated silver, and finished Ag/AgCl electrode after chloridization. Scale bar = 0.5 mm. (**B**) Potentiometric response of Ag/AgCl reference electrodes (n = 4) against commercial silver chloride electrode (Ag/AgCl 3 M NaCl). Electrolyte: 1 mM KNO_3 + 10 mM NaCl.

The dynamic response of the sensor (SCISE vs. electroplated Ag/AgCl) when subjected to alternating flow and static conditions showed that hydrodynamics did not exert much influence on the response. Results in Figure 4A show that at concentrations > 10^{-5} M, the potential differences (ΔE) between 0.45 mL/min flow and static phases were less than 3 mV. The influence was larger at low concentrations (<10^{-6} M), especially for the K^+ sensor which showed ΔE >20 mV and a much slower response in the static phase. These results can be explained by the leaching of primary ions (K^+ or NO_3^-) from the membrane that raised their local concentrations in the solution. On the other hand, the flow keeps the local concentration to the actual value by constantly refreshing the solution. Despite some flow

sensitivity, the sensors showed a generally rapid response (~20 s) to concentration changes (Figure 4A, inset).

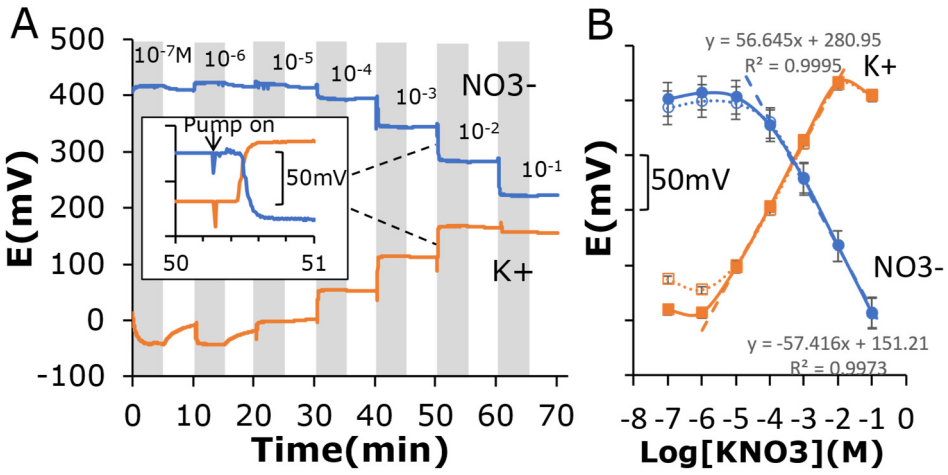

Figure 4. Potentiometric response of the multiplexed sensor (K^+ and NO_3^- electrodes and Ag/AgCl reference) in microchannel under alternating flow (shaded) and static conditions: (**A**) Real-time sensor response. Flow rate: 0.45 mL/min. Electrolyte: KNO_3 + 10 mM NaCl. Inset: enlarged view showing sensor's response to changing concentration. (**B**) Calibration curves of the NO_3^- and K^+ ISEs (3 electrodes for each ion). Solid lines indicate flow condition and dashed lines indicate static condition.

Both the K^+ and NO_3^- electrodes displayed near-Nernstian response over the three-decade concentration range, which covers typical ranges in biological and environmental samples. Figure 4B shows that the K^+ electrodes exhibited a slope of 56.6 mV/dec from 10^{-5} to 10^{-2} M, and the NO_3^- electrodes displayed −57.4 mV/dec from 10^{-4} to 10^{-1} M. The limits of detection (LOD) were calculated to be 1.9×10^{-6} M and 3.6×10^{-5} M for K^+ and NO_3^- electrodes, respectively, with the flow condition showing a slightly lower LOD than the static condition. With NaCl (10 mM) as the background electrolyte, selectivity (LogP) can also be derived and was determined to be −3.72 for the K^+ electrode (vs. Na^+) and −2.44 for the NO_3^- electrode (vs. Cl^-). These values agree with the results from capillary-based electrodes in the bulk solution [19], suggesting that neither the PCB substrate nor the adhesive tape affected sensor selectivity. In the upper range, the signal of K^+ electrodes eventually flat out beyond 10 mM due to the so-called co-ion interference of NO_3^- [30]. Further extension of the upper limit may be achieved by increasing the concentration of ionic sites (TPB) in the membrane.

Evaluation of the long-term performance showed that the sensors retained most of their sensitivity (95% for NO_3^- and 91% for K^+ ISEs) after 3 weeks (Figure 5A). The gradual decay may be linked to the leaching or breakdown of membrane ingredients (e.g., plasticizer or ionic sites), which was thought to have also resulted in decrease in sensor conductivity and capacitance [14]. In addition, the sensors have maintained their selectivity over the testing period, with the NO_3^- ISEs displaying selectivity coefficients of −2.4 to −2.5 (vs. Cl^-) and the K^+ ISEs of −3.7 to −4.2 (vs. Na^+) (Figure 5B). The maintenance of selectivity ensured that the sensors would function properly in complex samples. In terms of baseline (Figure 5C), the sensors showed an average drift of 6–11 mV per day (mV/d) in the first week and have stabilized since then with the drift typically below 3 mV/d. However, even with a drift of 3 mV/d, the error could be as high as 13% for daily measurement. Therefore, the sensors here would need regular calibration in the long term, especially for the first 2 weeks. For calibration-free sensors, drift on the order of μV/h was suggested [10].

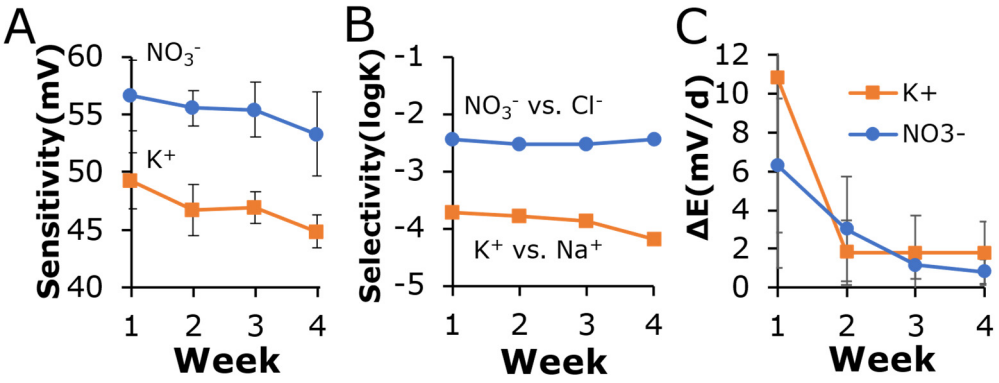

Figure 5. Long-term sensor performance: (**A**) Sensitivity of ISEs. The sensitivities were measured by two-point calibration between 1 and 10 mM KNO_3. (**B**) Selectivity of ISEs. For K^+ electrodes, selectivity was measured against Na^+ ions; for NO_3^- electrodes, selectivity was against Cl^- ions. (**C**). Baseline drift of ISEs at 1 mM KNO_3 (in mV per day, mV/d) over a 4-week period. Reference: electroplated Ag/AgCl. For all measurements, 10 mM NaCl was added as background. At least 3 electrodes were used for each measurement. Sensors were stored dry in air between measurements.

3.4. Self-Calibration and Plant Sap Test

To evaluate the sensor system for in situ measurements, the response of the sensor was measured in an automated two-point calibration (Figure 6). At each step, the sensor was measured for 60 s at default followed by solution switching for 25 s. These parameters were chosen to ensure complete rinsing of the channel while minimizing reagent consumption. The sample volume used for each measurement was ~187.5 µL. As shown in Figure 6, after about two calibrating cycles, both K^+ and NO_3^- sensors showed a highly reproducible response, with the K^+ ISEs exhibiting 20.4 ± 0.45 and 68.4 ± 0.45 mV for the last five cycles at 1 and 10 mM KNO_3, respectively, and the NO_3^- ISEs showing 299.1 ± 0.18 and 244.9 ± 0.36 mV. The high reproducibility indicates that the sensor system can robustly perform self-calibration.

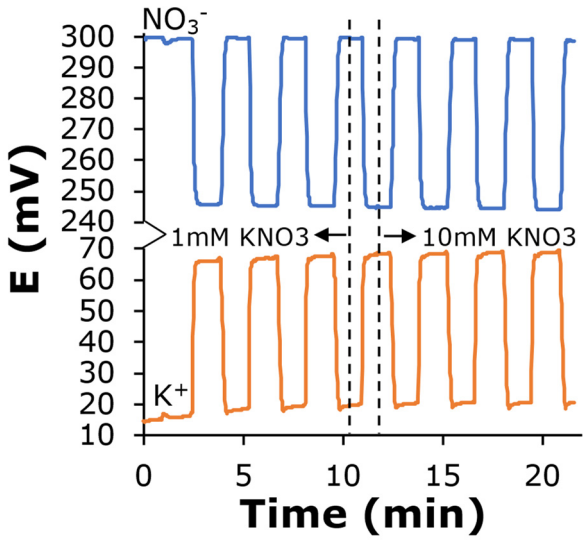

Figure 6. Automated two-point calibration. Potentials were recorded for 1 min at stopped-flow and then the channel was rinsed with a new solution for 25 s. Electrolyte: KNO_3 + 10 mM NaCl. Reference: electroplated Ag/AgCl.

The system was further applied to detect ionic nutrients in plant sap (*Z. mays*). As shown in Figure 7A, a program of pump and valve actions was implemented so that multiple sap samples were analyzed in a continuous manner and the sensors were calibrated before and after each sample. Based on the calibrations, the concentrations of K^+ and

NO_3^- in the original sap were calculated to be 1–20 mM (Figure 7B, Table 1), which were consistent with reported values in maize [15,31]. The low NO_3^- levels in some samples indicate that plants were most likely suffering from nitrogen deficiency. Moreover, the results of our sensors were consistent with that of commercial ISEs, with typical differences of ≤3 mM and correlation coefficients >0.95. The mean accuracy of our measurement against commercial sensors was 105.7% for K^+ ions. The NO_3^- sensor showed a small systematic bias (~ +1.3 mM), with respect to commercial sensors, possibly due to interference from Cl^- ions (which were suppressed in commercial ISEs with the use of an ionic strength adjustor). When such bias was corrected by subtraction, the adjusted mean accuracy of measurement was calculated to be 95.2% for NO_3^-.

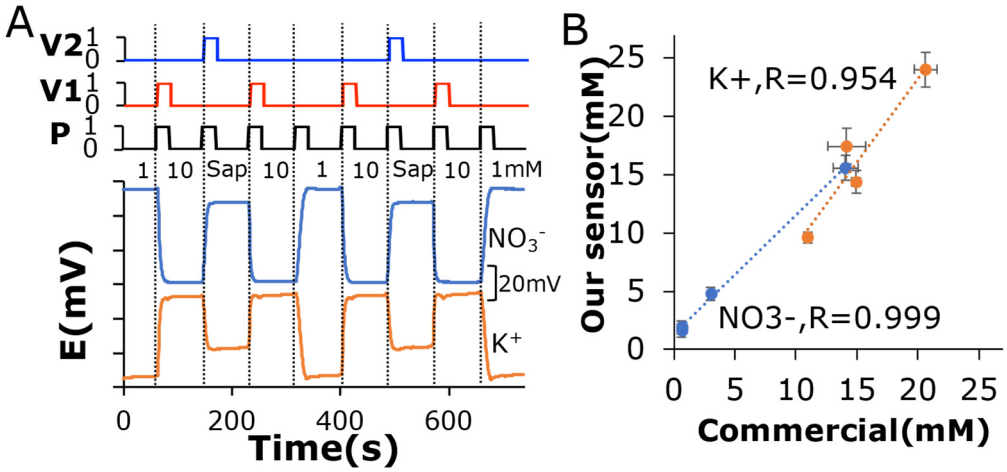

Figure 7. Xylem sap test: (**A**) Real-time sensor response in a programmed sequence of pump (P) and valves (V1,V2). The sensors were calibrated before and after each sap measurement with KNO_3 (1 and 10 mM) + NaCl. (**B**) Comparison of ion concentrations in original sap between our sensors and commercial ISEs. Sap samples were prediluted 10× with 1 mM KNO_3 (+ 10 mM NaCl) for our sensor and 10–20× for commercial ISEs.

Table 1. Concentrations of K^+ and NO_3^- ions in xylem sap (*Z. mays*) measured by our sensors and commercial ISEs (n is the number of measurements).

Sample	K^+_Our Sensor (mM)	K^+_Commercial (mM)	NO_3^-_Our Sensor (mM)	NO_3^-_Commercial (mM)
1	9.59 ± 0.48 (n = 16)	10.98 ± 0.15 (n = 3)	1.63 ± 0.57 (n = 16)	0.62 ± 0.19 (n = 3)
2	14.37 ± 0.98 (n = 16)	14.94 ± 0.34 (n = 3)	4.76 ± 0.56 (n = 16)	3.01 ± 0.2 (n = 3)
3	17.46 ± 1.5 (n = 4)	14.17 ± 1.59 (n = 4)	1.9 ± 0.52 (n = 4)	0.63 ± 0.23 (n = 4)
4	24.02 ± 1.52 (n = 8)	20.64 ± 0.92 (n = 8)	15.59 ± 1.05 (n = 12)	14.07 ± 1.03 (n = 8)

4. Conclusions

This work demonstrated a self-calibrating sensor system by integrating SCISEs with flow-control modules into the same readout circuit. The resulting sensor system is compact, cost-effective, and robust, with the potential for in situ measurements in a variety of agricultural, biomedical, environmental, or geochemical applications. In the future, the capability of the system can be further expanded. For example, the system currently supports multiplexed sensing of three ion analytes via USB-A interface; the number of analytes can be readily increased using an alternative electronic interface such as HDMI (16-pin) or USB-C (24-pin). At the same time, the sensors can be tailored to other ions by simply varying the selective components (ionophores/ion exchangers). In addition, a microcontroller unit can be integrated into the custom PCB circuit to further reduce the footprint of the electronics. Furthermore, chip-based potentiostat circuits can be integrated to enable other sensing schemes (e.g., amperometry or voltammetry). The fluid control

modules of the system can also be readily adapted into other analytical systems that require automated sensor calibration.

Author Contributions: Z.Z.: Conceptualization, Methodology, Investigation, Data Curation, Formal analysis, Visualization, Writing—Original Draft. E.B.: Investigation, Writing—Review and Editing. I.P.: Conceptualization, Supervision, Writing—Review and Editing. All authors have read and agreed to the published version of the manuscript.

Funding: This research was funded by the National Science Foundation and the industrial members of the Center for Advanced Design and Manufacturing of Integrated Microfluidics (NSF I/UCRC award IIP-1841473).

Institutional Review Board Statement: Not applicable.

Informed Consent Statement: Not applicable.

Data Availability Statement: The data that support the findings of this study are available from the corresponding author upon reasonable request.

Acknowledgments: We are grateful to Dylan Lynch at UIC Engineering Makerspace for assistance with the laser cutter, and Mark Lehman at 3M for tape samples.

Conflicts of Interest: The authors declare that they have no competing interests.

References

1. Nemiroski, A.; Christodouleas, D.; Hennek, J.W.; Kumar, A.; Maxwell, E.J.; Fernández-Abedul, M.; Whitesides, G.M. Universal mobile electrochemical detector designed for use in resource-limited applications. *Proc. Natl. Acad. Sci. USA* **2014**, *111*, 11984–11989. [CrossRef] [PubMed]
2. Lauks, I.R. Microfabricated Biosensors and Microanalytical Systems for Blood Analysis. *Acc. Chem. Res.* **1998**, *31*, 317–324. [CrossRef]
3. Sheikh, M.; Qassem, M.; Triantis, I.F.; Kyriacou, P.A. Advances in Therapeutic Monitoring of Lithium in the Management of Bipolar Disorder. *Sensors* **2022**, *22*, 736. [CrossRef] [PubMed]
4. Lynch, A.; Diamond, D.; Leader, M. Point-of-need diagnosis of cystic fibrosis using a potentiometric ion-selective electrode array. *Analyst* **2000**, *125*, 2264–2267. [CrossRef]
5. Gao, W.; Emaminejad, S.; Nyein, H.Y.Y.; Challa, S.; Chen, K.; Peck, A.; Fahad, H.M.; Ota, H.; Shiraki, H.; Kiriya, D.; et al. Fully integrated wearable sensor arrays for multiplexed in situ perspiration analysis. *Nature* **2016**, *529*, 509–514. [CrossRef]
6. Alizadeh, A.; Burns, A.; Lenigk, R.; Gettings, R.; Ashe, J.; Porter, A.; McCaul, M.; Barrett, R.; Diamond, D.; White, P.; et al. A wearable patch for continuous monitoring of sweat electrolytes during exertion. *Lab Chip* **2018**, *18*, 2632–2641. [CrossRef]
7. Huang, S.; Shih, W.; Chen, Y.; Wu, Y.; Chen, L. Ion composition profiling and pattern recognition of vegetable sap using a sol-id-contact ion-selective electrode array. *Biosens. Bioelectron.* **2021**, *9*, 100088.
8. Cuartero, M.; Crespo, G.A.; Cherubini, T.; Pankratova, N.; Confalonieri, F.; Massa, F.; Tercier-Waeber, M.-L.; Abdou, M.; Schaefer, J.; Bakker, E. In Situ Detection of Macronutrients and Chloride in Seawater by Submersible Electrochemical Sensors. *Anal. Chem.* **2018**, *90*, 4702–4710. [CrossRef]
9. Cuartero, M.; Pankratova, N.; Cherubini, T.; Crespo, G.A.; Massa, F.; Confalonieri, F.; Bakker, E. In Situ Detection of Species Relevant to the Carbon Cycle in Seawater with Submersible Potentiometric Probes. *Environ. Sci. Technol. Lett.* **2017**, *4*, 410–415. [CrossRef]
10. Rousseau, C.R.; Bühlmann, P. Calibration-free potentiometric sensing with solid-contact ion-selective electrodes. *TrAC Trends Anal. Chem.* **2021**, *140*, 116277. [CrossRef]
11. Calvo-López, A.; Puyol, M.; Casalta, J.; Alonso-Chamarro, J. Multi-parametric polymer-based potentiometric analytical microsystem for future manned space missions. *Anal. Chim. Acta* **2017**, *995*, 77–84. [CrossRef] [PubMed]
12. Ceresa, A.; Sokalski, T.; Pretsch, E. Influence of key parameters on the lower detection limit and response function of solvent polymeric membrane ion-selective electrodes. *J. Electroanal. Chem.* **2001**, *501*, 70–76. [CrossRef]
13. Lindner, E.; Gyurcsányi, R.; Buck, R. Tailored Transport Through Ion-Selective Membranes for Improved Detection Limits and Selectivity Coefficients. *Electroanalysis* **1999**, *11*, 695–702. [CrossRef]
14. Zhang, Z.; Papautsky, I. Solid Contact Ion-selective Electrodes on Printed Circuit Board with Membrane Displacement. *Electroanalysis* **2022**. [CrossRef]
15. Goodger, J.Q.D.; Sharp, R.E.; Marsh, E.L.; Schachtman, D.P. Relationships between xylem sap constituents and leaf conductance of well-watered and water-stressed maize across three xylem sap sampling techniques. *J. Exp. Bot.* **2005**, *56*, 2389–2400. [CrossRef]
16. Thermo Fisher Scientific. Potassium Ion Selective Electrode User Guide. Available online: www.thermofisher.com (accessed on 31 December 2022).
17. Laser, D.; Santiago, J. A review of micropumps. *J. Micromech. Microeng.* **2004**, *14*, R35–R64. [CrossRef]
18. Oh, K.; Ahn, C. A review of microvalves. *J. Micromech. Microeng.* **2006**, *16*, R13–R39. [CrossRef]

19. Zhang, Z.; Papautsky, I. Miniature Ion-selective Electrodes with Mesoporous Carbon Black as Solid Contact. *Electroanalysis* **2021**, *33*, 2143–2151. [CrossRef]
20. Merkel, T.; Graeber, M.; Pagel, L. A new technology for fluidic microsystems based on PCB technology. *Sens. Actuators A Phys.* **1999**, *77*, 98–105. [CrossRef]
21. Li, J.; Wang, Y.; Dong, E.; Chen, H. USB-driven microfluidic chips on printed circuit boards. *Lab Chip* **2013**, *14*, 860–864. [CrossRef]
22. Kontakis, K.; Petropoulos, A.; Kaltsas, G.; Speliotis, T.; Gogolides, E. A novel microfluidic integration technology for PCB-based devices: Application to microflow sensing. *Microelectron. Eng.* **2009**, *86*, 1382–1384. [CrossRef]
23. Burdallo, I.; Jimenez-Jorquera, C.; Fernández-Sánchez, C.; Baldi, A. Integration of microelectronic chips in microfluidic systems on printed circuit board. *J. Micromech. Microeng.* **2012**, *22*, 105022. [CrossRef]
24. Ghanim, M.H.; Abdullah, M.Z. Design of disposable DNA biosensor microchip with amperometric detection featuring PCB substrate. *BioChip J.* **2013**, *7*, 51–56. [CrossRef]
25. Marshall, L.A.; Wu, L.L.; Babikian, S.; Bachman, M.; Santiago, J.G. Integrated Printed Circuit Board Device for Cell Lysis and Nucleic Acid Extraction. *Anal. Chem.* **2012**, *84*, 9640–9645. [CrossRef] [PubMed]
26. Nath, P.; Fung, D.; Kunde, Y.A.; Zeytun, A.; Branch, B.; Goddard, G. Rapid prototyping of robust and versatile microfluidic components using adhesive transfer tapes. *Lab Chip* **2010**, *10*, 2286–2291. [CrossRef]
27. Bhattacharjee, N.; Urrios, A.; Kang, S.; Folch, A. The upcoming 3D-printing revolution in microfluidics. *Lab Chip* **2016**, *16*, 1720–1742. [CrossRef]
28. Moschou, D.; Trantidou, T.; Regoutz, A.; Carta, D.; Morgan, H.; Prodromakis, T. Surface and Electrical Characterization of Ag/AgCl Pseudo-Reference Electrodes Manufactured with Commercially Available PCB Technologies. *Sensors* **2015**, *15*, 18102–18113. [CrossRef]
29. Papamatthaiou, S.; Zupancic, U.; Kalha, C.; Regoutz, A.; Estrela, P.; Moschou, D. Ultra stable, inkjet-printed pseudo reference electrodes for lab-on-chip integrated electrochemical biosensors. *Sci. Rep.* **2020**, *10*, 17152. [CrossRef]
30. Bühlmann, P.; Amemiya, S.; Yajima, S.; Umezawa, Y. Co-Ion Interference for Ion-Selective Electrodes Based on Charged and Neutral Ionophores: A Comparison. *Anal. Chem.* **1998**, *70*, 4291–4303. [CrossRef]
31. Bahrun, A.; Jensen, C.; Asch, F.; Mogensen, V. Drought-induced changes in xylem pH, ionic composition, and ABA concentration act as early signals in field-grown maize (*Zea mays* L.). *J. Exp. Bot.* **2002**, *53*, 251–263. [CrossRef]